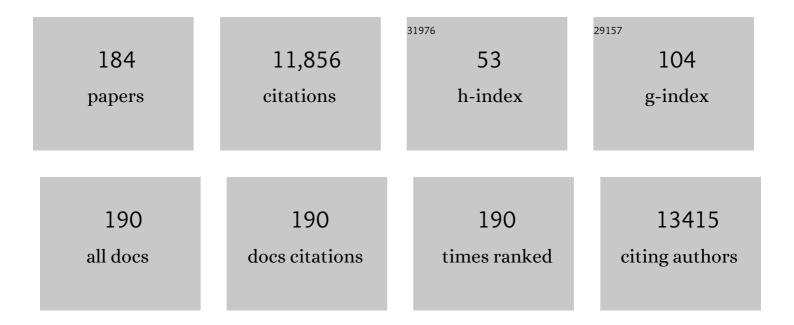
Zhaosheng Li

List of Publications by Year in descending order

Source: https://exaly.com/author-pdf/1491975/publications.pdf Version: 2024-02-01



7HAOSHENCLI

#	Article	IF	CITATIONS
1	Organics challenge inorganics for efficient photoelectrochemical water oxidation. Science Bulletin, 2022, 67, 226-228.	9.0	5
2	Effects of transition metal doping on electronic structure of metastable β-Fe ₂ O ₃ photocatalyst for solar-to-hydrogen conversion. Physical Chemistry Chemical Physics, 2022, 24, 6958-6963.	2.8	3
3	FeVO ₄ nanowires for efficient photocatalytic CO ₂ reduction. Catalysis Science and Technology, 2022, 12, 3289-3294.	4.1	12
4	Bandgap Engineering and Oxygen Vacancies of Ni _{<i>x</i>} V ₂ O _{5+<i>x</i>} (<i>x </i> = 1, 2, 3) for Efficient Visible Lightâ€Driven CO ₂ to CO with Nearly 100% Selectivity. Solar Rrl, 2022, 6, .	5.8	8
5	In situ optical spectroscopic understanding of electrochemical passivation mechanism on sol–gel processed WO3 photoanodes. Journal of Energy Chemistry, 2022, 71, 20-28.	12.9	17
6	A Waterâ€Soluble Highly Oxidizing Cobalt Molecular Catalyst Designed for Bioinspired Water Oxidation. Angewandte Chemie - International Edition, 2022, 61, .	13.8	13
7	Extraterrestrial photosynthesis by Chang'E-5 lunar soil. Joule, 2022, 6, 1008-1014.	24.0	15
8	Deactivation and Stabilization Mechanism of Photothermal CO ₂ Hydrogenation over Black TiO ₂ . ACS Sustainable Chemistry and Engineering, 2022, 10, 6382-6388.	6.7	16
9	Homogeneous solution assembled Turing structures with near zero strain semi-coherence interface. Nature Communications, 2022, 13, .	12.8	13
10	Ultrathin 3D radial tandem-junction photocathode with a high onset potential of 1.15 V for solar hydrogen production. Chinese Journal of Catalysis, 2022, 43, 1842-1850.	14.0	1
11	An energy level alignment strategy to boost the open-circuit voltage via a Mg:TiO2 compact layer in the planar heterojunction CsPbBr3 solar cells. Applied Physics Letters, 2022, 120, .	3.3	5
12	Centimeter-scale perovskite SrTaO2N single crystals with enhanced photoelectrochemical performance. Science Bulletin, 2022, 67, 1458-1466.	9.0	6
13	A2V2O7 (A = Co, Ni, Cu and Zn) for CO2 reduction under visible-light irradiation: Effects of A site replacement. Applied Catalysis B: Environmental, 2022, 317, 121722.	20.2	10
14	Exploring N-Containing Compound Catalyst for H2S Selective Oxidation: Case Study of TaON and Ta3N5. Catalysis Letters, 2021, 151, 1728-1737.	2.6	2
15	Evaluating the promotional effects of WO3 underlayers in BiVO4 water splitting photoanodes. Chemical Engineering Journal, 2021, 417, 128095.	12.7	27
16	A strategy of asymmetric local structure based on mesoporous MoO ₂ toward efficient electrocatalysis. Chemical Communications, 2021, 57, 7834-7837.	4.1	3
17	Synthesis of porous Au–Ag alloy nanorods with tunable plasmonic properties and intrinsic hotspots for surface-enhanced Raman scattering. CrystEngComm, 2021, 23, 3467-3476.	2.6	6
18	Photocatalytic and Thermocatalytic Conversion of Methane. Solar Rrl, 2021, 5, 2000596.	5.8	16

#	Article	IF	CITATIONS
19	Ureaâ€Assisted Synthesis and Tailoring Cobalt Cores for Synergetic Promotion of Hydrogen Evolution Reaction in Acid and Alkaline Media. Advanced Energy and Sustainability Research, 2021, 2, 2000091.	5.8	5
20	Promotion effect of metal phosphides towards electrocatalytic and photocatalytic water splitting. EcoMat, 2021, 3, e12097.	11.9	46
21	Material Design and Surface/Interface Engineering of Photoelectrodes for Solar Water Splitting. Solar Rrl, 2021, 5, 2100100.	5.8	33
22	An ultraviolet-ozone post-treatment to remove the inherent impurities in all-ambient solution-processed CsPbBr3 perovskite films. Applied Physics Letters, 2021, 118, 221604.	3.3	5
23	Suppressing the Defects in CsPbI2Br Perovskite Photovoltaic Films via a Homogeneous Cap-Mediated Annealing Strategy. Energy & Fuels, 2021, 35, 11488-11495.	5.1	4
24	Extraterrestrial artificial photosynthetic materials for <i>in-situ</i> resource utilization. National Science Review, 2021, 8, nwab104.	9.5	17
25	Direct Molecule Substitution Enabled Rapid Transformation of Wet PbBr ₂ (DMF) Precursor Films to CsPbBr ₃ Perovskite. ACS Applied Energy Materials, 2021, 4, 6414-6421.	5.1	7
26	2D Highâ€Entropy Hydrotalcites. Small, 2021, 17, e2103412.	10.0	27
27	Metastable-phase β-Fe2O3 photoanodes for solar water splitting with durability exceeding 100 h. Chinese Journal of Catalysis, 2021, 42, 1992-1998.	14.0	16
28	Lanthanum bismuth oxide photocatalysts for CO ₂ reduction to CO with high selectivity. Sustainable Energy and Fuels, 2021, 5, 2688-2694.	4.9	6
29	Carrier Mobility Enhancement in (121)-Oriented CsPbBr ₃ Perovskite Films Induced by the Microstructure Tailoring of PbBr ₂ Precursor Films. ACS Applied Electronic Materials, 2021, 3, 373-384.	4.3	30
30	Cooperative catalysis coupling photo-/photothermal effect to drive Sabatier reaction with unprecedented conversion and selectivity. Joule, 2021, 5, 3235-3251.	24.0	91
31	State-of-the-art advancements of crystal facet-exposed photocatalysts beyond TiO2: Design and dependent performance for solar energy conversion and environment applications. Materials Today, 2020, 33, 75-86.	14.2	97
32	Non-oxide semiconductors for artificial photosynthesis: Progress on photoelectrochemical water splitting and carbon dioxide reduction. Nano Today, 2020, 30, 100830.	11.9	76
33	Photocatalysis: an overview of recent developments and technological advancements. Science China Chemistry, 2020, 63, 149-181.	8.2	107
34	Curing the fundamental issue of impurity phases in two-step solution-processed CsPbBr3 perovskite films. Science Bulletin, 2020, 65, 726-737.	9.0	34
35	Modulation of Disordered Coordination Degree Based on Surface Defective Metal–Organic Framework Derivatives toward Boosting Oxygen Evolution Electrocatalysis. Small, 2020, 16, e2003630.	10.0	44
36	Sol-gel synthesis of highly reproducible WO3 photoanodes for solar water oxidation. Science China Materials, 2020, 63, 2261-2271.	6.3	12

#	Article	IF	CITATIONS
37	Phase degradation of all-inorganic perovskite CsPbI2Br films induced by a p-type CuI granular capping layer. Science China Materials, 2020, 63, 2487-2496.	6.3	9
38	Paving the road toward the use of β-Fe2O3 in solar water splitting: Raman identification, phase transformation and strategies for phase stabilization. National Science Review, 2020, 7, 1059-1067.	9.5	38
39	Effects of oxygen impurity concentration on the interfacial properties of Ta3N5/Ta5N6 composite photoelectrode: A DFT calculation. Applied Catalysis B: Environmental, 2020, 278, 119296.	20.2	6
40	Suppression of Point Defects for Band Edge Engineering in a Semiconducting Photocatalyst. Journal of Physical Chemistry Letters, 2020, 11, 1708-1713.	4.6	11
41	Simultaneous Optimization of Phase and Morphology of CsPbBr 3 Films via Controllable Ostwald Ripening by Ethylene Glycol Monomethylether/Isopropanol Biâ€Solvent Engineering. Advanced Engineering Materials, 2020, 22, 2000162.	3.5	19
42	Molecular-level understanding of the deactivation pathways during methanol photo-reforming on Pt-decorated TiO2. Applied Catalysis B: Environmental, 2020, 272, 118980.	20.2	17
43	Polaron States as a Massive Electron-Transfer Pathway at Heterojunction Interface. Journal of Physical Chemistry Letters, 2020, 11, 9184-9194.	4.6	14
44	<i>In situ</i> preparation of Bi ₂ S ₃ nanoribbon-anchored BiVO ₄ nanoscroll heterostructures for the catalysis of Cr(<scp>vi</scp>) photoreduction. Catalysis Science and Technology, 2020, 10, 3843-3847.	4.1	14
45	Elegant Molecular Iodine/Antisolvent Solution Engineering To Tune the Fermi Level of Perovskite CH ₃ NH ₃ PbI ₃ . ACS Applied Energy Materials, 2019, 2, 5753-5758.	5.1	7
46	Effect of Bulk Hydrogen on the Photocatalytic Activity of Semiconducting Ta ₃ N ₅ : A Hybrid-DFT Viewpoint. Journal of Physical Chemistry C, 2019, 123, 28763-28768.	3.1	7
47	Defect Engineering in Semiconductors: Manipulating Nonstoichiometric Defects and Understanding Their Impact in Oxynitrides for Solar Energy Conversion. Advanced Functional Materials, 2019, 29, 1808389.	14.9	56
48	Construction of silica-encapsulated gold-silver core-shell nanorod: Atomic facets enrichment and plasmon enhanced catalytic activity with high stability and reusability. Materials and Design, 2019, 177, 107837.	7.0	21
49	Design Principles for Construction of Charge Transport Channels in Particle-Assembled Water-Splitting Photoelectrodes. ACS Sustainable Chemistry and Engineering, 2019, 7, 10509-10515.	6.7	13
50	Highly symmetrical, 24-faceted, concave BiVO ₄ polyhedron bounded by multiple high-index facets for prominent photocatalytic O ₂ evolution under visible light. Chemical Communications, 2019, 55, 4777-4780.	4.1	29
51	Interfacial Effects on the Band Edges of Ta3N5 Photoanodes in an Aqueous Environment: A Theoretical View. IScience, 2019, 13, 432-439.	4.1	10
52	BiVO ₄ tubular structures: oxygen defect-rich and largely exposed reactive {010} facets synergistically boost photocatalytic water oxidation and the selective Nî€N coupling reaction of 5-amino-1 <i>H</i> -tetrazole. Chemical Communications, 2019, 55, 5635-5638.	4.1	17
53	Charge compensation doping to improve the photocatalytic and photoelectrochemical activities of Ta3N5: A theoretical study. Applied Catalysis B: Environmental, 2019, 244, 502-510.	20.2	24
54	Heterogeneous degradation of organic contaminants in the photo-Fenton reaction employing pure cubic β-Fe2O3. Applied Catalysis B: Environmental, 2019, 245, 410-419.	20.2	107

#	Article	IF	CITATIONS
55	Reactive Inorganic Vapor Deposition of Perovskite Oxynitride Films for Solar Energy Conversion. Research, 2019, 2019, 9282674.	5.7	17
56	Surface states as electron transfer pathway enhanced charge separation in TiO2 nanotube water splitting photoanodes. Applied Catalysis B: Environmental, 2018, 234, 100-108.	20.2	77
57	High Energy Density Asymmetric Supercapacitor Based ZnS/NiCo ₂ S ₄ /Co ₉ S ₈ Nanotube Composites Materials. Advanced Materials Interfaces, 2018, 5, 1800018.	3.7	54
58	Interfacial Engineering of Hierarchical Transition Metal Oxide Heterostructures for Highly Sensitive Sensing of Hydrogen Peroxide. Small, 2018, 14, e1703713.	10.0	40
59	Insight into the influence of high temperature annealing on the onset potential of Ti-doped hematite photoanodes for solar water splitting. Chinese Chemical Letters, 2018, 29, 791-794.	9.0	6
60	Tuning spontaneous polarization to alter water oxidation/reduction activities of LiNbO3. Applied Physics Letters, 2018, 112, .	3.3	11
61	Rational design of electrocatalysts for simultaneously promoting bulk charge separation and surface charge transfer in solar water splitting photoelectrodes. Journal of Materials Chemistry A, 2018, 6, 2568-2576.	10.3	56
62	Promoted photoelectrochemical activity of BiVO4 coupled with LaFeO3 and LaCoO3. Research on Chemical Intermediates, 2018, 44, 1013-1024.	2.7	10
63	Improving solar water-splitting performance of LaTaON2 by bulk defect control and interface engineering. Applied Catalysis B: Environmental, 2018, 226, 111-116.	20.2	26
64	Theoretical Insight into Charge-Recombination Center in Ta ₃ N ₅ Photocatalyst: Interstitial Hydrogen. Journal of Physical Chemistry C, 2018, 122, 489-494.	3.1	9
65	Tandem photoelectrochemical cells for solar water splitting. Advances in Physics: X, 2018, 3, 1487267.	4.1	25
66	Exploring facile strategies for high-oxidation-state metal nitride synthesis: carbonate-assisted one-step synthesis of Ta3N5 films for solar water splitting. Science Bulletin, 2018, 63, 1404-1410.	9.0	19
67	Facet-Dependent Enhancement in the Activity of Bismuth Vanadate Microcrystals for the Photocatalytic Conversion of Methane to Methanol. ACS Applied Nano Materials, 2018, 1, 6683-6691.	5.0	79
68	Improved water-splitting performances of CuW1â^'xMoxO4 photoanodes synthesized by spray pyrolysis. Science China Materials, 2018, 61, 1297-1304.	6.3	22
69	Galvanic cell reaction driven electrochemical doping of TiO2 nanotube photoanodes for enhanced charge separation. Chemical Communications, 2018, 54, 11116-11119.	4.1	3
70	Effects of Mg–Zr codoping on the photoelectrochemical properties of a Ta ₃ N ₅ semiconductor: a theoretical insight. Journal of Materials Chemistry A, 2017, 5, 6966-6973.	10.3	19
71	Selective Electrochemical Detection of Dopamine on Polyoxometalateâ€Based Metal–Organic Framework and Its Composite with Reduced Graphene Oxide. Advanced Materials Interfaces, 2017, 4, 1601241.	3.7	51
72	Oxygen-Impurity-Induced Direct–Indirect Band Gap in Perovskite SrTaO ₂ N. Journal of Physical Chemistry C, 2017, 121, 6864-6867.	3.1	14

#	Article	IF	CITATIONS
73	A beta-Fe ₂ O ₃ nanoparticle-assembled film for photoelectrochemical water splitting. Dalton Transactions, 2017, 46, 10673-10677.	3.3	27
74	A novel wide-spectrum response hexagonal YFeO ₃ photoanode for solar water splitting. RSC Advances, 2017, 7, 18418-18420.	3.6	18
75	Current advances in MoS2/semiconductor heterojunction with enhanced photocatalytic activity. Current Opinion in Green and Sustainable Chemistry, 2017, 6, 42-47.	5.9	10
76	A facile spray pyrolysis method to prepare Ti-doped ZnFe ₂ O ₄ for boosting photoelectrochemical water splitting. Journal of Materials Chemistry A, 2017, 5, 7571-7577.	10.3	113
77	Two-dimensional nanomaterials for photocatalytic CO ₂ reduction to solar fuels. Sustainable Energy and Fuels, 2017, 1, 1875-1898.	4.9	156
78	Bi ₂ MoO ₆ Nanostrip Networks for Enhanced Visibleâ€Light Photocatalytic Reduction of CO ₂ to CH ₄ . ChemPhysChem, 2017, 18, 3240-3244.	2.1	38
79	Improved charge separation efficiency of hematite photoanodes by coating an ultrathin p-type LaFeO ₃ overlayer. Nanotechnology, 2017, 28, 394003.	2.6	9
80	Back Electron Transfer at TiO ₂ Nanotube Photoanodes in the Presence of a H ₂ O ₂ Hole Scavenger. ACS Applied Materials & Interfaces, 2017, 9, 33887-33895.	8.0	31
81	Threeâ€Ðimensional Hierarchical Architectures Derived from Surfaceâ€Mounted Metal–Organic Framework Membranes for Enhanced Electrocatalysis. Angewandte Chemie - International Edition, 2017, 56, 13781-13785.	13.8	193
82	Enhanced solar photocurrent of LaTaON ₂ photoanodes via electrochemical treatment. IOP Conference Series: Materials Science and Engineering, 2017, 182, 012007.	0.6	2
83	Threeâ€Dimensional Hierarchical Architectures Derived from Surfaceâ€Mounted Metal–Organic Framework Membranes for Enhanced Electrocatalysis. Angewandte Chemie, 2017, 129, 13969-13973.	2.0	42
84	Compensation of band-edge positions in titanium-doped <mml:math xmlns:mml="http://www.w3.org/1998/Math/MathML"> <mml:mrow> <mml:msub> <mml:mi> Ta </mml:mi> <mml:m mathvariant="normal">N <mml:mn> 5 </mml:mn> </mml:m </mml:msub> </mml:mrow> photoanode for enhanced water splitting performance: A first-principles insight. Physical Review</mml:math 	nn>32.4	nl:mn> 11
85	Materials, 2017, 1, . Hydrogen Evolution Reaction of γ-Mo0.5W0.5 C Achieved by High Pressure High Temperature Synthesis. Catalysts, 2016, 6, 208.	3.5	3
86	Enhanced InGaN/GaN photoelectrodes for visibleâ€lightâ€driven hydrogen generation by surface roughening. Physica Status Solidi (A) Applications and Materials Science, 2016, 213, 2704-2708.	1.8	1
87	A perspective on perovskite oxide semiconductor catalysts for gas phase photoreduction of carbon dioxide. MRS Communications, 2016, 6, 216-225.	1.8	18
88	Formation of Hierarchical Structure Composed of (Co/Ni)Mn-LDH Nanosheets on MWCNT Backbones for Efficient Electrocatalytic Water Oxidation. ACS Applied Materials & Interfaces, 2016, 8, 14527-14534.	8.0	155
89	Enhanced Waterâ€5plitting Performance of Perovskite SrTaO ₂ N Photoanode Film through Ameliorating Interparticle Charge Transport. Advanced Functional Materials, 2016, 26, 7156-7163.	14.9	86
90	Layered crystalline ZnIn ₂ S ₄ nanosheets: CVD synthesis and photo-electrochemical properties. Nanoscale, 2016, 8, 18197-18203.	5.6	42

#	Article	IF	CITATIONS
91	Photoelectrochemical cell for unassisted overall solar water splitting using a BiVO ₄ photoanode and Si nanoarray photocathode. RSC Advances, 2016, 6, 9905-9910.	3.6	64
92	Theoretical study on the surface stabilities, electronic structures and water adsorption behavior of the Ta ₃ N ₅ (110) surface. Physical Chemistry Chemical Physics, 2016, 18, 7938-7945.	2.8	8
93	Significant improvements in InGaN/GaN nano-photoelectrodes for hydrogen generation by structure and polarization optimization. Scientific Reports, 2016, 6, 20218.	3.3	27
94	Enhancement of Photoelectrochemical Performance in Water Oxidation over Bismuth Vanadate Photoanodes by Incorporation with Reduced Graphene Oxide. ChemCatChem, 2015, 7, 2979-2985.	3.7	11
95	Unraveling the mechanism of 720 nm sub-band-gap optical absorption of a Ta ₃ N ₅ semiconductor photocatalyst: a hybrid-DFT calculation. Physical Chemistry Chemical Physics, 2015, 17, 8166-8171.	2.8	34
96	Effects of oxygen impurities and nitrogen vacancies on the surface properties of the Ta ₃ N ₅ photocatalyst: a DFT study. Physical Chemistry Chemical Physics, 2015, 17, 23265-23272.	2.8	19
97	Enhanced Performance of Photoelectrochemical Water Splitting with ITO@α-Fe ₂ O ₃ Core–Shell Nanowire Array as Photoanode. ACS Applied Materials & Interfaces, 2015, 7, 26482-26490.	8.0	60
98	Construction of Visible-Light-Responsive SrTiO3 with Enhanced CO2 Adsorption Ability: Highly Efficient Photocatalysts for Artifical Photosynthesis. Catalysis Letters, 2015, 145, 640-646.	2.6	29
99	Application of binder-free TiOxN1â^'x nanogrid film as a high-power supercapacitor electrode. Journal of Power Sources, 2015, 296, 53-63.	7.8	25
100	Solar fuel production: Strategies and new opportunities with nanostructures. Nano Today, 2015, 10, 468-486.	11.9	126
101	A hybrid density functional theory study of the anion distribution and applied electronic properties of the LaTiO ₂ N semiconductor photocatalyst. Physical Chemistry Chemical Physics, 2015, 17, 19631-19636.	2.8	11
102	Photocatalytic CO2 reduction of BaCeO3 with 4f configuration electrons. Applied Surface Science, 2015, 358, 463-467.	6.1	27
103	Barium zirconate: a new photocatalyst for converting CO ₂ into hydrocarbons under UV irradiation. Catalysis Science and Technology, 2015, 5, 1758-1763.	4.1	44
104	Geâ€Mediated Modification in Ta ₃ N ₅ Photoelectrodes with Enhanced Charge Transport for Solar Water Splitting. Chemistry - A European Journal, 2014, 20, 16384-16390.	3.3	38
105	Quantitative Analysis and Visualized Evidence for High Charge Separation Efficiency in a Solidâ€Liquid Bulk Heterojunction. Advanced Energy Materials, 2014, 4, 1301785.	19.5	88
106	Effects of Ba–O codoping on the photocatalytic activities of Ta ₃ N ₅ photocatalyst: a DFT study. RSC Advances, 2014, 4, 55615-55621.	3.6	9
107	Highly Photoâ€Responsive LaTiO ₂ N Photoanodes by Improvement of Charge Carrier Transport among Film Particles. Advanced Functional Materials, 2014, 24, 3535-3542.	14.9	166
108	MnO2 nanolayers on highly conductive TiO0.54N0.46 nanotubes for supercapacitor electrodes with high power density and cyclic stability. Physical Chemistry Chemical Physics, 2014, 16, 8521.	2.8	21

#	Article	IF	CITATIONS
109	Basic Molten Salt Route to Prepare Porous SrTiO ₃ Nanocrystals for Efficient Photocatalytic Hydrogen Production. European Journal of Inorganic Chemistry, 2014, 2014, 3731-3735.	2.0	19
110	Role of oxygen impurity on the mechanical stability and atomic cohesion of Ta ₃ N ₅ semiconductor photocatalyst. Physical Chemistry Chemical Physics, 2014, 16, 15375-15380.	2.8	37
111	Cathodic shift of onset potential for water oxidation on a Ti ⁴⁺ doped Fe ₂ O ₃ photoanode by suppressing the back reaction. Energy and Environmental Science, 2014, 7, 752-759.	30.8	228
112	Photoelectrochemical water oxidation of LaTaON2 under visible-light irradiation. International Journal of Hydrogen Energy, 2014, 39, 7697-7704.	7.1	53
113	Effects of oxygen doping on optical band gap and band edge positions of Ta3N5 photocatalyst: A GGA+U calculation. Journal of Catalysis, 2014, 309, 291-299.	6.2	67
114	Improvement in photocatalytic H2 evolution over g-C3N4 prepared from protonated melamine. Applied Surface Science, 2014, 295, 253-259.	6.1	119
115	Enhanced luminescence intensity of Sr3B2O6:Eu2+ phosphor prepared by sol–gel method. Journal of Alloys and Compounds, 2013, 579, 432-437.	5.5	20
116	A Coâ€catalyst‣oaded Ta ₃ N ₅ Photoanode with a High Solar Photocurrent for Water Splitting upon Facile Removal of the Surface Layer. Angewandte Chemie - International Edition, 2013, 52, 11016-11020.	13.8	208
117	Efficient red phosphor double-perovskite Ca3WO6 with A-site substitution of Eu3+. Dalton Transactions, 2013, 42, 13502.	3.3	39
118	Theoretical study of water adsorption and dissociation on Ta3N5(100) surfaces. Physical Chemistry Chemical Physics, 2013, 15, 16054.	2.8	28
119	A transparent Ti4+ doped hematite photoanode protectively grown by a facile hydrothermal method. CrystEngComm, 2013, 15, 2386.	2.6	42
120	Photoelectrochemical cells for solar hydrogen production: current state of promising photoelectrodes, methods to improve their properties, and outlook. Energy and Environmental Science, 2013, 6, 347-370.	30.8	969
121	Formation energy and photoelectrochemical properties of BiVO ₄ after doping at Bi ³⁺ or V ⁵⁺ sites with higher valence metal ions. Physical Chemistry Chemical Physics, 2013, 15, 1006-1013.	2.8	138
122	Tunable orange red phosphors: S ^{2â^'} -doped high temperature phase Ca ₃ SiO ₄ Cl ₂ :Eu ²⁺ for solid-state lighting. RSC Advances, 2013, 3, 1965-1969.	3.6	12
123	Zinc Gallogermanate Solid Solution: A Novel Photocatalyst for Efficiently Converting CO ₂ into Solar Fuels. Advanced Functional Materials, 2013, 23, 1839-1845.	14.9	89
124	Highly efficient visible light photocatalytic activity of Cr–La codoped SrTiO3 with surface alkalinization: An insight from DFT calculation. Computational Materials Science, 2013, 79, 87-94.	3.0	19
125	An efficient charge compensated red phosphor Sr3WO6: K+, Eu3+ – For white LEDs. Journal of Alloys and Compounds, 2013, 553, 221-224.	5.5	50
126	Na adsorption on SrTiO3 (0 0 1) surface and its interaction with water: A DFT calculation. Applied Surface Science, 2013, 270, 359-363.	6.1	6

#	Article	IF	CITATIONS
127	Water Adsorption and Decomposition on N/V-Doped Anatase TiO ₂ (101) Surfaces. Journal of Physical Chemistry C, 2013, 117, 6172-6184.	3.1	24
128	Nearly Monodispersed LiNbO ₃ Nanocrystals Synthesized by a Nonaqueous Sol–Gel Process and Their Photocatalytic H ₂ Evolution Activities. European Journal of Inorganic Chemistry, 2013, 2013, 4142-4145.	2.0	10
129	An Ionâ€Exchange Phase Transformation to ZnGa ₂ O ₄ Nanocube Towards Efficient Solar Fuel Synthesis. Advanced Functional Materials, 2013, 23, 758-763.	14.9	72
130	Semiconductors for Photoelectrochemical Hydrogen Generation. , 2013, , 201-232.		0
131	Innenrücktitelbild: A Co-catalyst-Loaded Ta3N5Photoanode with a High Solar Photocurrent for Water Splitting upon Facile Removal of the Surface Layer (Angew. Chem. 42/2013). Angewandte Chemie, 2013, 125, 11381-11381.	2.0	0
132	Firstâ€Principles Calculations on Electronic Structures of N/Vâ€Doped and Nâ€Vâ€Dodoped Anatase TiO ₂ (101) Surfaces. ChemPhysChem, 2012, 13, 3836-3847.	2.1	21
133	Reconstruction of the (001) surface of TiO2 nanosheets induced by the fluorine-surfactant removal process under UV-irradiation for dye-sensitized solar cells. Physical Chemistry Chemical Physics, 2012, 14, 4763.	2.8	40
134	A facile strategy to passivate surface states on the undoped hematite photoanode for water splitting. Electrochemistry Communications, 2012, 23, 41-43.	4.7	43
135	A Theoretical Study of Water Adsorption and Decomposition on the Low-Index Stoichiometric Anatase TiO ₂ Surfaces. Journal of Physical Chemistry C, 2012, 116, 7430-7441.	3.1	70
136	Effects of Surface Electrochemical Pretreatment on the Photoelectrochemical Performance of Mo-Doped BiVO ₄ . Journal of Physical Chemistry C, 2012, 116, 5076-5081.	3.1	172
137	A dye-free photoelectrochemical solar cell based on BiVO4 with a long lifetime of photogenerated carriers. Electrochemistry Communications, 2012, 22, 49-52.	4.7	21
138	Interfacial modification of photoelectrode in ZnO-based dye-sensitized solar cells and its efficiency improvement mechanism. RSC Advances, 2012, 2, 7708.	3.6	26
139	Efficient visible-light-driven photocatalytic H2 production over Cr/N-codoped SrTiO3. International Journal of Hydrogen Energy, 2012, 37, 12120-12127.	7.1	90
140	ZnO plates synthesized from the ammonium zinc nitrate hydroxide precursor. CrystEngComm, 2012, 14, 154-159.	2.6	34
141	Structure and Properties of Water on the Anatase TiO ₂ (101) Surface: From Single-Molecule Adsorption to Interface Formation. Journal of Physical Chemistry C, 2012, 116, 11054-11061.	3.1	64
142	Co ₃ O ₄ Nanoparticles as Robust Water Oxidation Catalysts Towards Remarkably Enhanced Photostability of a Ta ₃ N ₅ Photoanode. Advanced Functional Materials, 2012, 22, 3066-3074.	14.9	205
143	Two-step reactive template route to a mesoporous ZnGaNO solid solution for improved photocatalytic performance. Journal of Materials Chemistry, 2011, 21, 5682.	6.7	29
144	Structure and energetics of low-index stoichiometric monoclinic clinobisvanite BiVO4 surfaces. RSC Advances, 2011, 1, 874.	3.6	58

#	Article	IF	CITATIONS
145	Remarkable enhancement in photocurrent of In0.20Ga0.80N photoanode by using an electrochemical surface treatment. Applied Physics Letters, 2011, 99, .	3.3	27
146	BiVO4 nano–leaves: Mild synthesis and improved photocatalytic activity for O2 production under visible light irradiation. CrystEngComm, 2011, 13, 2500.	2.6	65
147	Solvothermal synthesis of monodisperse iron oxides with various morphologies and their applications in removal of Cr(vi). CrystEngComm, 2011, 13, 2727.	2.6	25
148	Solar hydrogen generation from seawater with a modified BiVO4 photoanode. Energy and Environmental Science, 2011, 4, 4046.	30.8	564
149	Electronic structure and optical properties of monoclinic clinobisvanite BiVO4. Physical Chemistry Chemical Physics, 2011, 13, 4746.	2.8	327
150	Sol–gel hydrothermal synthesis of visible-light-driven Cr-doped SrTiO3 for efficient hydrogen production. Journal of Materials Chemistry, 2011, 21, 11347.	6.7	157
151	Facile temperature-controlled synthesis of hexagonal Zn2GeO4nanorods with different aspect ratios toward improved photocatalytic activity for overall water splitting and photoreduction of CO2. Chemical Communications, 2011, 47, 5632-5634.	4.1	159
152	Enhanced Incident Photon-to-Electron Conversion Efficiency of Tungsten Trioxide Photoanodes Based on 3D-Photonic Crystal Design. ACS Nano, 2011, 5, 4310-4318.	14.6	267
153	Microwave Hydrothermal Synthesis, Structural Characterization, and Visible-Light Photocatalytic Activities of Single-Crystalline Bismuth Ferric Nanocrystals. Journal of the American Ceramic Society, 2011, 94, 2688-2693.	3.8	75
154	Surface modification of hematite photoanode films with rhodium. Rare Metals, 2011, 30, 38-41.	7.1	6
155	Understanding the interaction of water with anatase TiO2 (101) surface from density functional theory calculations. Physics Letters, Section A: General, Atomic and Solid State Physics, 2011, 375, 2939-2945.	2.1	27
156	Design and theoretical analysis of resonant cavity for second-harmonic generation with high efficiency. Applied Physics Letters, 2011, 98, 031102.	3.3	9
157	Modulation of dendrite growth of cuprous oxide by electrodeposition. Journal of Crystal Growth, 2010, 312, 3085-3090.	1.5	16
158	Density functional theory study of doping effects in monoclinic clinobisvanite BiVO4. Physics Letters, Section A: General, Atomic and Solid State Physics, 2010, 374, 4919-4927.	2.1	95
159	Improved hydrogen evolution activities under visible light irradiation over NaTaO3 codoped with lanthanum and chromium. Materials Chemistry and Physics, 2010, 121, 506-510.	4.0	69
160	Growth of Inâ€rich and Gaâ€rich InGaN alloys by MOCVD and fabrication of InGaNâ€based photoelectrodes. Physica Status Solidi C: Current Topics in Solid State Physics, 2010, 7, 1817-1820.	0.8	16
161	An orthophosphate semiconductor with photooxidation properties under visible-lightÂirradiation. Nature Materials, 2010, 9, 559-564.	27.5	1,807
162	Synthesis of a mesoporous single crystal Ga2O3 nanoplate with improved photoluminescence and high sensitivity in detecting CO. Chemical Communications, 2010, 46, 6388.	4.1	54

#	Article	IF	CITATIONS
163	Surface properties and electronic structure of low-index stoichiometric anatase TiO ₂ surfaces. Journal of Physics Condensed Matter, 2010, 22, 175008.	1.8	54
164	Facile synthesis of anatase TiO2 mesocrystal sheets with dominant {001} facets based on topochemical conversion. CrystEngComm, 2010, 12, 3425.	2.6	54
165	Improved photoelectrochemical responses of Si and Ti codoped α-Fe2O3 photoanode films. Applied Physics Letters, 2010, 97, .	3.3	105
166	Facile Method To Synthesize Mesoporous Multimetal Oxides (ATiO ₃ , A = Sr, Ba) with Large Specific Surface Areas and Crystalline Pore walls. Chemistry of Materials, 2010, 22, 1276-1278.	6.7	45
167	Effect of crystal growth on mesoporous Pb3Nb4O13 formation, and their photocatalytic activity under visible-light irradiation. Journal of Materials Chemistry, 2010, 20, 2865.	6.7	19
168	Enhancement in Luminescence of Naln(WO[sub 4])[sub 2] via Bismuth Doping. Journal of the Electrochemical Society, 2010, 157, P63.	2.9	2
169	Synthesis, growth mechanism and photoelectrochemical properties of BiVO ₄ microcrystal electrodes. Journal Physics D: Applied Physics, 2010, 43, 405402.	2.8	41
170	Increasing the Oxygen Vacancy Density on the TiO ₂ Surface by La-Doping for Dye-Sensitized Solar Cells. Journal of Physical Chemistry C, 2010, 114, 18396-18400.	3.1	166
171	Forced Impregnation Approach to Fabrication of Large-Area, Three-Dimensionally Ordered Macroporous Metal Oxides. Chemistry of Materials, 2010, 22, 3583-3585.	6.7	53
172	Polymerizable complex synthesis of BaZr1â^'xSnxO3 photocatalysts: Role of Sn4+ in the band structure and their photocatalytic water splitting activities. Journal of Materials Chemistry, 2010, 20, 6772.	6.7	52
173	Effective electron collection in highly (110)-oriented ZnO porous nanosheet framework photoanode. Nanotechnology, 2010, 21, 065703.	2.6	45
174	Enhancement in Photoluminescence of CaMoO[sub 4]:Eu[sup 3+] Through Introducing MVO[sub 4] (M=Y or Bi). Journal of the Electrochemical Society, 2009, 156, J367.	2.9	2
175	Luminescence properties of Sr2ZnWO6:Eu3+ phosphors. Journal of Alloys and Compounds, 2009, 469, L6-L9.	5.5	56
176	Photooxidation of Polycyclic Aromatic Hydrocarbons over NaBiO3 under Visible Light Irradiation. Catalysis Letters, 2008, 122, 131-137.	2.6	31
177	Correlation of Crystal Structures, Electronic Structures, and Photocatalytic Properties in a Series of Ag-based Oxides:  AgAlO ₂ , AgCrO ₂ , and Ag ₂ CrO ₄ . Journal of Physical Chemistry C, 2008, 112, 3134-3141.	3.1	152
178	Stable response to visible light of InGaN photoelectrodes. Applied Physics Letters, 2008, 92, 262110.	3.3	50
179	Correlation between the band positions of (SrTiO3)1â^'x·(LaTiO2N)x solid solutions and photocatalytic properties under visible light irradiation. Physical Chemistry Chemical Physics, 2008, 10, 6717.	2.8	104
180	Enhancement of photoelectric conversion properties of SrTiO3/α-Fe2O3heterojunction photoanode. Journal Physics D: Applied Physics, 2007, 40, 3925-3930.	2.8	57

#	Article	IF	CITATIONS
181	Photocatalytic properties of MIn(WO4)2 (M = Li, Na, and K). Journal of Materials Research, 2007, 22, 958-964.	2.6	5
182	Enhanced activity of mesoporous Nb2O5 for photocatalytic hydrogen production. Applied Surface Science, 2007, 253, 8500-8506.	6.1	173
183	Degradation in photocatalytic activity induced by hydrogen-related defects in nano-LiNbO3 material. Applied Physics Letters, 2006, 88, 071917.	3.3	47
184	In situ growth of epitaxial lead iodide films composed of hexagonal single crystals. Journal of Materials Chemistry, 2005, 15, 4555.	6.7	87